Environmental Earth Sciences (2019) 78:47
https://doi.org/10.1007/s12665-018-8003-4

ORIGINAL ARTICLE

Multi-hazard assessment modeling via multi-criteria analysis and GIS: a case study

Hariklia D. Skilodimou[1] · George D. Bathrellos[1] · Konstantinos Chousianitis[2] · Ahmed M. Youssef[3] · Biswajeet Pradhan[4,5]

Received: 14 May 2018 / Accepted: 17 December 2018 / Published online: 7 January 2019

Abstract

Multi-hazard assessment modeling comprises an essential tool in any plan that aims to mitigate the impact of future natural disasters. For a particular area they can be generated by combining assessment maps for different types of natural hazards. In the present study, the analytical hierarchy process (AHP) supported by a Geographical Information System (GIS) was utilized to initially produce assessment maps on hazards from landslides, floods and earthquakes and subsequently to combine them into a single multi-hazard map. Evaluation of the reliability of the proposed model predictions was performed through uncertainty analysis of the variables that we used for producing the final model. The drainage basin of Peneus (Pinios) River (Western Peloponnesus, Greece), an area that is prone to landslides, floods and seismic events, was selected for the implementation of the aforementioned approach. Our findings revealed that the high hazard zones are mainly distributed in the western and north-eastern part of the region under investigation. The calculated multi-hazard map, which corresponds to the potential urban development suitability map of the study area, was classified into five classes, namely of very low, low, moderate, high and very high suitability. The most suitable areas for urban development are distributed mostly in the eastern part, in agreement with the low and very low hazard level for the three considered natural hazards. In addition, by performing uncertainty analysis we showed that the spatial distribution of the suitability zones does not change significantly. Ultimately, the final map was verified using the actual inventory of landslides and floods that affected the study area. In this context, we showed that 80% of the landslide occurrences and all the recorded flood events fall within the boundaries of the moderate, low and very low suitability zones. Consequently, the predictive capacity of the applied method is quite good. Finally, the spatial distribution of the urban areas and the road network were compared with the derived suitability map and the results revealed that approximately 50% of both of them are located within areas susceptible to natural hazards. The proposed approach can be useful for engineers, planners and local authorities in spatial planning and natural hazard management.

Keywords Analytical hierarchy process · Natural hazard assessment maps · Suitability map for urban development · Peneus River, Western Peloponnesus, Greece

✉ George D. Bathrellos
gbathrellos@geol.uoa.gr

Hariklia D. Skilodimou
hskilodimou@geol.uoa.gr

Konstantinos Chousianitis
chousianitis@noa.gr

Ahmed M. Youssef
amyoussef70@yahoo.com

Biswajeet Pradhan
Biswajeet.Pradhan@uts.edu.au; biswajeet24@gmail.com

[1] Department of Geography and Climatology, Faculty of Geology and Geoenvironment, National and Kapodistrian University of Athens, University Campus, 15784 Zografou, Athens, Greece

[2] Institute of Geodynamics, National Observatory of Athens, 11810 Lofos Nymfon, Athens, Greece

[3] Department of Geology, Faculty of Science, Sohag University, 82524 Sohag, Egypt

[4] The Centre for Advanced Modelling and Geospatial Information Systems (CAMGIS), Faculty of Engineering and Information Technology, University of Technology Sydney, Ultimo, NSW 2007, Australia

[5] Department of Energy and Mineral Resources Engineering, Sejong University, Choongmu-gwan, 209 Neungdong-roGwangjin-gu, Seoul 05006, Republic of Korea

Introduction

Natural hazard events are able to significantly affect the natural and artificial environment. In this context, the change of landforms due to natural disasters have the potential to affect and, in some cases, even to restrict the human interaction with the ecosystem (Skilodimou et al. 2014; Bathrellos et al. 2014, 2017a, b, c).To minimize fatalities and reduce the economic impact that accompanies their occurrence, a proper planning is crucial. Accordingly, reliable information on the spatial distribution of natural disasters comprise a key tool when environmental planners and engineers are trying to select suitable sites for land use development (Abdulwahid and Pradhan 2016; Althuwaynee and Pradhan 2016; Bathrellos et al. 2009; Chousianitis et al. 2016; Das et al. 2013; Hopkins 1977; Jebur et al. 2015; Pham et al. 2016; Rozos et al. 2013; Skilodimou et al. 2003; Slaymaker 1997; Youssef et al. 2015).

Up until recently, and due to the fact that natural hazards are complex phenomena, the vast majority of the published studies have focused on the detailed examination of a single hazard phenomenon. However, a specific area usually is not affected solely by one natural hazard, but two or more have the ability to act at the same time or consecutively. In this context, the utilization of one hazard map for each type of natural disaster can become unmanageable when multiple hazard types have to be taken into account (Bender 1991). The solution to this difficulty is the adoption of multi-hazard analysis, which, enhanced with GIS-based methods that support a straightforward analysis of different kind of data, has been reliably used to develop natural hazard models and form the basis for vulnerability and risk management (El Morjani et al. 2007; F.E.M.A. 2004; Kappes et al. 2011; Schmidt et al. 2011).

Land use planning and suitability analysis can be performed by means of various heuristic, statistical, and deterministic approaches (e.g., Ayalew and Yamagishi 2005; Bathrellos et al. 2008; Papadopoulou-Vrynioti et al. 2014; Svoray et al. 2005; Tsolaki-Fiaka et al. 2018). Saaty (1977) developed the analytical hierarchy processes (AHP), a multiple objective decision making approach, which is among the most widely applied deterministic methods. It is a weight evaluation process which takes into account qualitative and quantitative parameters and ultimately results in the assessment of alternative solutions to a particular problem, among which the best solution is able to be identified (Saaty 1990, 2004). This method has been commonly combined with GIS for the assessment of a single natural hazard in local and regional scales (Fernández and Lutz 2010; Karaman and Erden 2014; Peng et al. 2012; Pourghasemi et al. 2012) as well as for performing land use suitability evaluation (Baja et al. 2007; Bathrellos et al. 2012; Panagopoulos et al. 2012; Thapa and Murayama 2008; Youssef et al. 2011). Although highly accepted within the scientific community, the AHP approach has some drawbacks such as the lack of uncertainty estimation (Bathrellos et al. 2013; Nefeslioglu et al. 2013).

Within the framework of the present paper, we implemented a multi-hazard approach considering landslide, flood and seismic hazard so as to ultimately evaluate and specify the appropriate locations for urban development. In the first stage, we adopted the AHP method which we combined with GIS to facilitate a consistent processing and handling of the different datasets and we created three hazard assessment maps. In the second stage the three maps obtained previously were further evaluated via the AHP method and lead to the final multi-hazard zonation map where the appropriate areas for urban development were identified. To account for uncertainties, we carried out sensitivity analysis in our hazard maps. Finally, the spatial extent of the urban areas as well as the road network was compared with the obtained suitability map.

Materials and methods

Study area

As a case study, we chose the region of the Peneus River basin, which is located at western Greece and specifically at western Peloponnesus (Fig. 1). This region has been frequently affected from different hazard phenomena including landslides, floods, and earthquakes. The basin of Peneus River occupies approximately 900 km^2 and is elongated along an E–W direction. It is a low altitude area, where the relief is characterized by gentle slopes, while only a small part of the basin is mountainous. The Peneus River flows towards the west and its drainage network is irregular probably due to its tectonic origin. The climate of the study area is mainly Mediterranean with annual precipitation ranging from 1200 to 1600 mm in the mountainous part and from 800 to 1200 mm in the lowlands.

The geological formations consist of both Neocene and Quaternary deposits along with alpine formations belonging to the Gavrovo and the Olonos-Pindos geotectonic zones. The formations of the Gavrovo zone are mainly flysch, while those of the Olonos-Pindos zone are sedimentary rocks which originate from a remnant ocean basin that formed during mid-Triassic (Migiros 2010). According to the latest Greek Seismic Code (EPPO 2003), the country was divided into three zones of seismic hazard on the basis of peak horizontal acceleration on "rock" sites (i.e., soil category B according to UBC) for 475 years mean return period. As per this classification, the study area falls into zone II where the

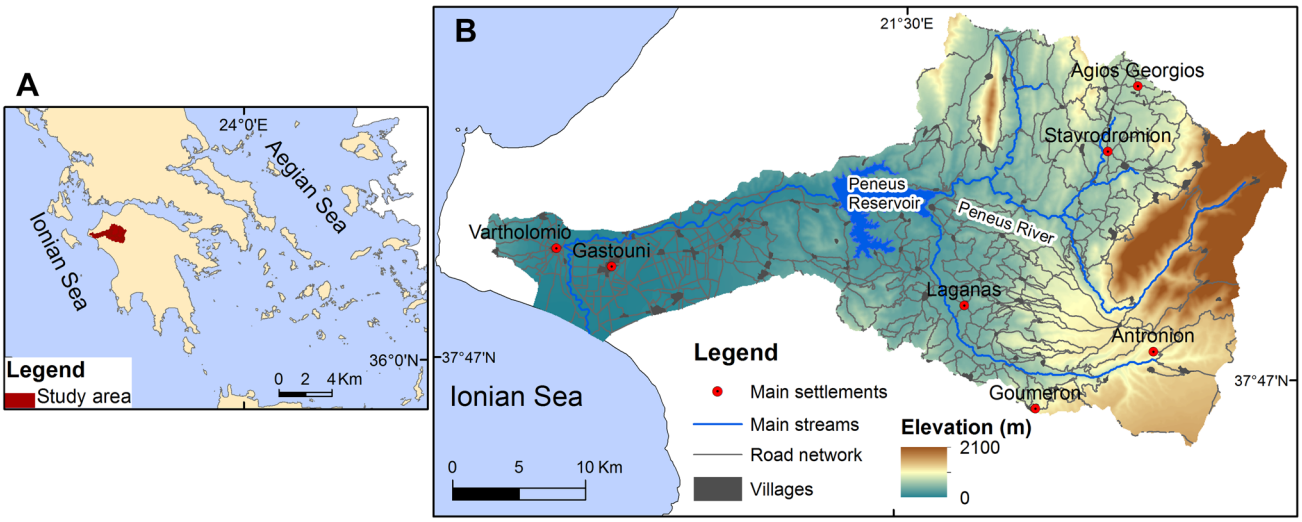

Fig. 1 **a** Map of Greece showing the location of the study area, **b** digital elevation Model, drainage and road networks and main settlements of the study area

maximum expected horizontal acceleration was estimated to be 0.24 g.

Materials

To create the three hazard maps, we used the following data:

- The topographic maps of the Hellenic Army Geographical Service (scale 1:50,000; H.A.G.S 1989);
- The geological maps of the Institute of Geology and Mineral Exploration (scale 1:500,000; I.G.M.E. 1983);
- The engineering geological map of the Institute of Geology and Mineral Exploration (scale 1:500,000; I.G.M.E. 1993);
- The precipitation data from seventeen (17) stations operated by: (1) the Ministry for the Environment, (2) the Hellenic National Meteorological Service, and (3) the Ministry of Agriculture;
- The landslides and the flood events which have been occurred within the study area. This dataset has been compiled using information from national databases as well as from related bibliography (Agricultural University of Athens 2007; Chalkias et al. 2016; Migiros 2010; Ministry of Environment and Energy 2017).

To facilitate the accurate processing and support the robust interaction between the above data, we created a spatial database.

The AHP method

The landslide, flood and seismic hazard assessment maps were produced using several factors. The weighting coefficients for the selected factors that were considered for the assessment of the three geohazards were calculated by applying the AHP, which is a quantitative and multi-criteria method that was designed for the hierarchical representation of a decision-making problem (Saaty 1977, 2006). The first step during the implementation of this method is the formation of the pair-wise comparison matrix whose entries reflect the relative significance of one factor compared to the others. The latter is measured using a nine point scale with the following levels of importance: 1 = equal, 3 = moderately, 5 = strongly, 7 = very strongly, 9 = extremely and 2, 4, 6, 8 = Intermediate values. In reverse, less important variables were valued from 1 to 1/9 (Saaty 1977). The consistency of each matrix after the calculation of the weight values was verified by means of the Consistency Ratio (CR):

$$CR = CI/RI$$

where RI is the random index whose value depends on the order of the matrix. The Consistency Index (CI) equals to:

$$CI = \lambda_{max} - n/n - 1$$

where λ_{max} is the largest eigenvalue of the matrix of order n. The CR is used so as to check and, therefore, avoid possible inconsistencies in the judgment matrix. Saaty (1990) justified that when the CR is below 0.1, the weighting coefficients are suitable, while if it is above 0.1, a reconsideration of the judgments is required to ensure realistic results. In the present study we compiled four matrices: three for evaluating the landslide, flood and seismic hazard and one for assessing the suitable regions for urban development. The pair-wise comparisons as well as the calculation of the weights and the consistency ratios were carried out using the Expert Choice 11 software (ECI 2004).

Individual hazard assessment maps

Landslide hazard assessment map

As stated previously, landslides have regularly caused damage to the urban areas and to the road network of the study area. The factors that were considered for the implementation of the landslide susceptibility model are lithology, distance from active faults, slope, precipitation, land use, distance from roads, and distance from streams. The selection of the aforementioned factors has been based on valuable knowledge from previous studies (Ayalew and Yamagishi 2005; Bathrellos et al. 2009; Althuwaynee and Pradhan 2016; Skilodimou et al. 2018). These factors were divided into classes corresponding to specific stability conditions. The number of classes and their values were picked on the basis of already published research (Rozos et al. 2011; Bathrellos et al. 2017a). Each class was standardized to a uniform rating scale, where the values ranged from 0 to 4. The 0 class represents the most stable conditions, i.e., reflecting negligible landslide hazard, while the 4 class implies major landslide hazard and corresponds to the most favourable conditions for slope failure (Table 1). Previous studies (Bathrellos et al. 2009, 2012; Rozos et al. 2011, 2013, 2017a) and personal experience were used as a basis to determine the assigned values for each class of the factors.

Lithology

The published geological map of the study area was the basis for the selection of the lithology classes (IGME 1983, 1993). Some of the geological formations were unified on the basis of their engineering performance in slope instability. As a result, the final lithology map included eight classes, namely (a) Quaternary loose mainly fine grained deposits, (b) Quaternary loose mixed phases deposits, (c) Quaternary coherent mixed phases deposits, (d) Quaternary coherent coarse-grained deposits, (e) Neocene coarse-grained sediments, (f) Neocene mixed phases sediments, (g) flysch, and (h) rocks (Fig. 2a). Among them, the Neocene mixed phases sediments along with flysch comprise the most prone lithology for landslide occurrence, and therefore, the higher rate was assigned.

Distance from active faults The active faults of the study area were assembled from already published papers (e.g., Koukouvelas et al. 1996; Goldsworthy and Jackson 2001; Goldsworthy et al. 2002; Kamberis et al. 2012; Kokinou et al. 2015). After digitizing the active faults, we created buffer zones at distances of 50 m, 100 m, 150 m and 200 m. Hence, five classes were used, that is (a) nearest (0–50 m), (b) very near (51–100 m), (c) near (101–150 m), (d) moderate distant (151–200 m) and (e) distant (> 200 m) (Fig. 2b). The most landslide prone class where we assigned the highest rate, is the nearest buffer zone.

Slope The slope thematic map was created using a digital elevation model (DEM) which was created from the topographic map of the study area (20 m contour interval). The slope map was classified into the following classes: (a) 0°–5°, (b) 6°–15°, (c) 16°–30°, (d) 31°–45°, and (e) > 45° (Fig. 2c). The highest rate was given to the latter class due to the fact that it is the most landslide prone category (Table 1).

Precipitation The precipitation map was generated using measurements from the meteorological stations located in the vicinity of the study area. The Inverse Distance Weighted (IDW) approach was adapted to interpolate the precipitation data. According to Setianto and Triandini, (2013), the IDW is an intuitive and efficient interpolation method, and it is recommended for data such as precipitation. The continuous values of the precipitation map were classified into: (a) < 800 mm, (b) 800–1000 mm, (c) 1000–1200 mm, (d) 1200–1400, and (e) > 1400 mm (Fig. 2d). The highest rate was given to the two classes where precipitation exceeds 1200 mm (Table 1).

Land use The land use data from the CORINE 2012 Land Cover (CLC) map and from Copernicus Program (Copernicus 2016) were used. The data published by the European Commission covers Europe at a scale of 1:100,000 and includes the corresponding class descriptions. The land uses of the study area were: (a) urban areas, (b) croplands, (c) woodlands, (d) shrublands together with grasslands, (e) sparsely vegetated areas along with bare lands, and (f) water areas (Fig. 3a). Cultivated areas are strongly related to landslide activity (Skilodimou et al. 2018) and therefore, the highest rank was given to the croplands (Table 1).

Distance from roads The road network was derived by digitizing the topographic maps of the study area (scale 1:50,000). As demonstrated in Rozos et al. (2011) the artificial and natural slope parts around the roads are prone to landslides. For that reason, we created buffer zones around the road network and the corresponding classes that we considered were (a) nearest (0–50 m), (b) very near (51–100 m), (c) near (101–150 m), (d) moderate distant (151–200 m) and (e) distant (> 200 m) (Fig. 3b). According to Skilodimou et al. (2018) the closer the distance is to the road network, the higher is the correlation with landslide manifestation. Consequently, the highest rank was assigned for distances less than 50 m, i.e., the "nearest" class (Table 1).

Distance from streams The drainage network of the study area was derived from the corresponding topographic maps and the streams were classified according to the Strahler's

Table 1 The factors and their classes that were considered for the assessment of landslide hazard, along with the corresponding rating for each one

Factor	Class	Rating
Lithology	Quaternary loose, mixed phases deposits	3
	Quaternary loose mainly fine grained deposits	3
	Quaternary coherent, mixed phases deposits	3
	Quaternary coherent, coarse-grained deposits	2
	Neocene coarse-grained sediments	1
	Neocene mixed phases sediments	4
	Flysch	4
	Rocks	0
Distance from faults (m)	< 50	4
	51–100	3
	101–150	2
	151–200	1
	> 200	0
Slope (°)	0–5	0
	6–15	1
	16–30	2
	31–45	3
	> 45	4
Precipitation (mm)	< 800	2
	800–1000	3
	1000–1200	3
	1200–1400	4
	> 1400	4
Land use	Urban areas	1
	Cropland	4
	Woodland	2
	Shrubland and grassland	3
	Sparsely vegetated areas and bare land	1
	Water areas	0
Distance from roads (m)	< 50	4
	51–100	3
	101–150	2
	151–200	1
	> 200	0
Distance from streams (m)	< 50	4
	51–100	3
	101–150	2
	151–200	1
	> 200	0

(1957) method. The hydrographic axes of the third and fourth order streams can be considered as principal factors for the occurrence of landslides. We created buffer zones at distances of 50 m, 100 m, 150 m and 200 m and established five classes that were are: (a) nearest (0–50 m), (b) very near (51–100 m), (c) near (101–150 m), (d) moderate distant (151–200 m) and (e) distant (> 200 m) (Fig. 3c). Like in the case of the active faults and the road network, the highest rank was assigned to the class with distances 0–50 m (Table 1).

With the AHP approach we achieved the cross-correlation of the adopted factors towards deriving the corresponding weights that were assigned to each factor separately. Firstly, we created a 7 × 7 matrix where we appended the values regarding the pair-wise comparisons between the factors affecting landslide occurrence. These values were derived after each co-author compiled the 7 × 7 matrix according to their options about the relative importance amongst the factors. These five separate matrices were subsequently combined using the average mean to produce the final matrix

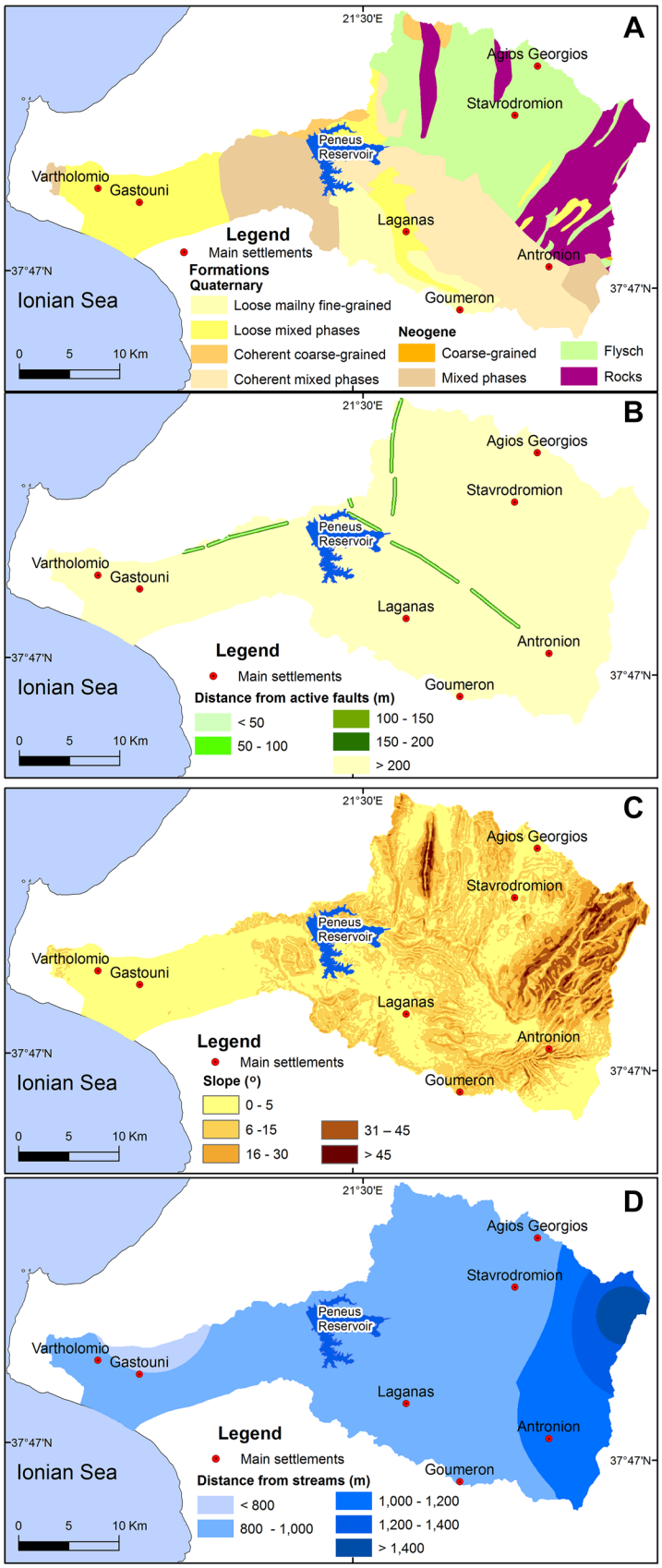

Fig. 2 Thematic maps of lithology (**a**), distance from active faults (**b**), slope (**c**) and precipitation (**d**) that were used in landslide hazard analysis

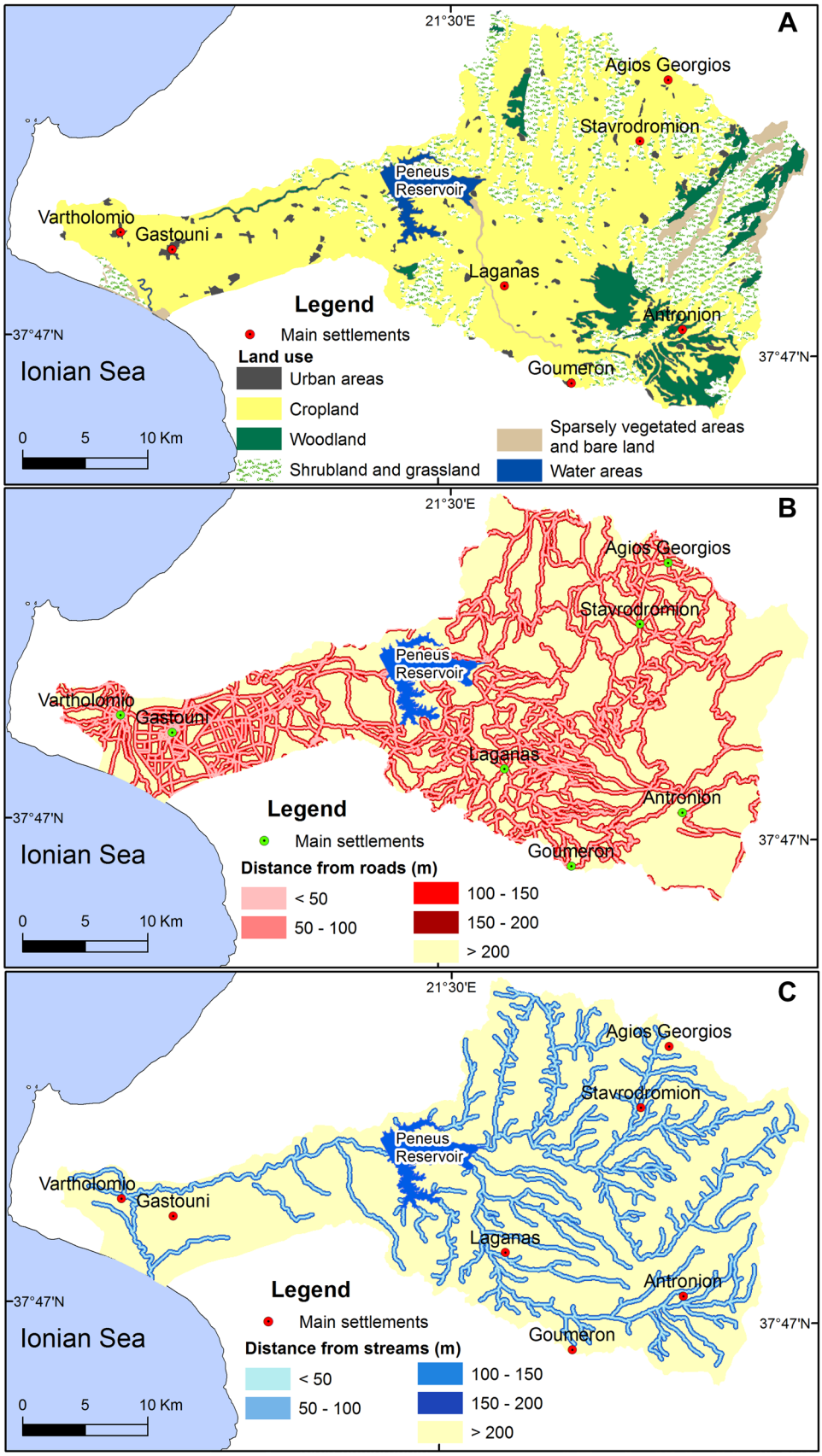

Fig. 3 Thematic maps of land use (**a**), distance from road network (**b**) and distance from streams (**c**) that were used in the assessment of landslide hazard

which is shown in Table 2. The central and eastern part of the study area is mainly characterized by relatively steep slopes (16°–30°) and steep slopes (> 30°) (Fig. 2c). These slopes have a greater chance of landsliding, while numerous landslides are located in the above mentioned parts of the study area. Therefore, we assigned the larger relative importance to the slope. On the other hand, in these parts of the study area there are woodlands and shrublands, which are poorly related to landslide occurrences. Thus, we assigned the lower relative importance to the land use. Finally, the application of the AHP provided the final weights for each factor. The pair-wise comparisons and the weighting coefficient of each adopted factor are tabulated in Table 2. After producing the corresponding matrix and the correlation of the principal factors, we validated the consistency ratio (CR) which was found to be 0.03 highlighting that according to Saaty (1990) the judgments shown in Table 2 were well assessed.

We estimated the overall score of the landslide hazard assessment by means of the weighted linear combination method according to the following equation:

$$\mathrm{LI} = \sum_{i=1}^{n} R_i W_i,$$

where LI corresponds to the landslide hazard index, n is the number of the factors, R_i is the rating of factor i and W_i is the weight of factor i. After employing the aforementioned equation, the landslide hazard assessment map was finally produced.

Using information included in national databases as well as from the literature (Agricultural University of Athens 2007; Migiros 2010), the landslide activity of the study area was specified. The landslide occurrences were validated on the basis of fieldwork and aerial photograph (scale 1:40,000) interpretation (Chalkias et al. 2016). These occurrences were used to compile an inventory which was subsequently utilized for the verification of the landslide hazard and multi-hazard maps.

Flood hazard assessment map

Flood susceptibility mapping can be performed via hydraulic-hydrodynamic models (i.e., Merwade et al. 2008; Migiros et al. 2011; Tehrany et al. 2015; Youssef et al. 2016), albeit such approaches require datasets that are usually not available at a watershed scale (de Moel et al. 2009). On the other hand, the AHP method has been commonly used for the delineation of flood prone areas, since this approach warrants accurate and reliable predictions (i.e., Rahmati et al. 2016).

In the present study, the selection of the factors that we incorporated in the AHP, the classes as well as their boundary values were selected on the basis of already published work (Stefanidis and Stathis 2013; Bathrellos et al. 2016, 2017a, 2018; Rahmati et al. 2016) as well as data availability. Accordingly, we considered elevation, slope, hydro-lithology, distance from streams, and land use. The precipitation records of the examined area referred to mean annual or monthly total precipitation without giving information about the rainfall intensity regime. In Table 3 the selected factors, their classes and their ratings are tabulated, and as in the case of the landslide hazard assessment, 4 represents the most favourable condition for the development of a flood event, while 0 the least favourable. As in the case of the landslide assessment, previous studies (Bathrellos et al. 2016, 2017a, 2018) as well as personal experience were used as a basis to determine the assigned values for each class of the considered factors.

Slope The slope thematic map was created using the DEM of the study area. Five classes were considered, that is (a) < 2°, (b) 3°–6°, (c) 7°–12°, (d) 13°–20° and (e) > 20° (Fig. 4a). According to Bathrellos et al. (2018) gentle slopes create favourable conditions for flooding and, therefore, the highest rate was assigned to the class with slope values < 2° (Table 3).

Table 2 Pair-wise comparisons, weighting coefficients of each adopted factor, and the estimated CR value

	L1	L2	L3	L4	L5	L6	L7	Weights, W_i
L1	1	2	1/3	1/2	3	2	3	0.157
L2		1	1/3	1/2	2	1	1	0.089
L3			1	2	5	3	4	0.321
L4				1	4	3	2	0.203
L5					1	1/3	1/3	0.044
L6						1	1/2	0.083
L7							1	0.100
CR = 0.03								

L1 lithology, *L2* distance from active faults, *L3* slope, *L4* precipitation, *L5* land use, *L6* distance from roads, *L7* distance from streams

Table 3 The factors and their classes that were considered for the assessment of flood hazard, along with the corresponding rating for each one

Factor	Class	Rating
Slope (°)	< 2	4
	3–6	3
	7–12	2
	13–20	1
	> 20	0
Elevation (m a.s.l.)	< 50	4
	51–100	3
	101–200	2
	201–500	1
	> 500	0
Distance from streams (m)	3rd order stream	
	0–50	4
	51–100	3
	101–150	2
	151–200	1
	> 200	0
	4th order stream	
	0–100	4
	101–200	3
	201–300	2
	301–400	1
	> 400	0
	5th order stream	
	0–100	4
	101–200	3
	201–400	2
	401–600	1
	> 600	0
	6th order stream	
	0–100	4
	101–300	3
	301–500	2
	501–700	1
	> 700	0
	7th order stream	
	0–100	4
	101–300	3
	301–600	2
	601–1,000	1
	> 1000 m	0
Hydrolithological formations	Impermeable	4
	Semi-permeable	3
	Permeable	2
Land use	Urban areas	4
	Cropland	2
	Woodland	0
	Shrubland and grassland	1
	Sparsely vegetated areas and bare land	3
	Water areas	4

Elevation Elevation is an important parameter for a reliable flood hazard assessment, because it controls the run-off direction movement along with the inundation extent and the water depth in case of a flood event. The DEM of the study area was used to create the elevation map, which, on the basis of the morphology, was subdivided into the following classes: (a) < 50 m a.s.l., (b) 50–100 m a.s.l., (c) 100–200 m a.s.l., (d) 200–500 m a.s.l., and (e) > 500 m a.s.l. (Fig. 4b; Table 3). Since lowland morphology is highly prone to flooding (Bathrellos et al. 2018), we assigned the highest rate to the class corresponding to elevation values below 50 m a.s.l.

Distance from streams In the previous section we classified the streams using the Strahler's (1957) approach and defined the drainage basin of Peneus River as a seventh order stream. As regards the flood hazard, due to the fact that the first and second order steams make a small contribution to flooding, we took into account only the streams of third and higher order. Based on previous published work (Bathrellos et al. 2016, 2017a) we created buffer zones of 50 m, 100 m, 150 m and 200 m around third order streams, of 100 m, 200 m, 300 m and 400 m around fourth order streams, of 100 m, 200 m, 400 m and 600 m around fifth order streams, of 100 m, 300 m, 500 m and 700 m around sixth order streams, and at distances of 100 m, 300 m, 600 m and 1000 m around the seventh order streams (Fig. 4c). According to Bathrellos et al. (2016), the closer the distance is to the drainage network, the higher is the correlation with flood occurrences. Thus, we assigned the highest rate to the buffer zone that encloses the nearest distances (Table 3).

Hydrolithology So as to categorize the geological formations, we took into account their corresponding hydrolithological behaviour and classified them into (a) permeable formations (limestones), (b) semi-permeable formations (loose to semi-coherent Quaternary and Neocene deposits), and (c) impermeable formations (flysch and coherent Neocene sediments). We assigned the highest rate to impermeable formations since they affect the quality and rate of infiltration

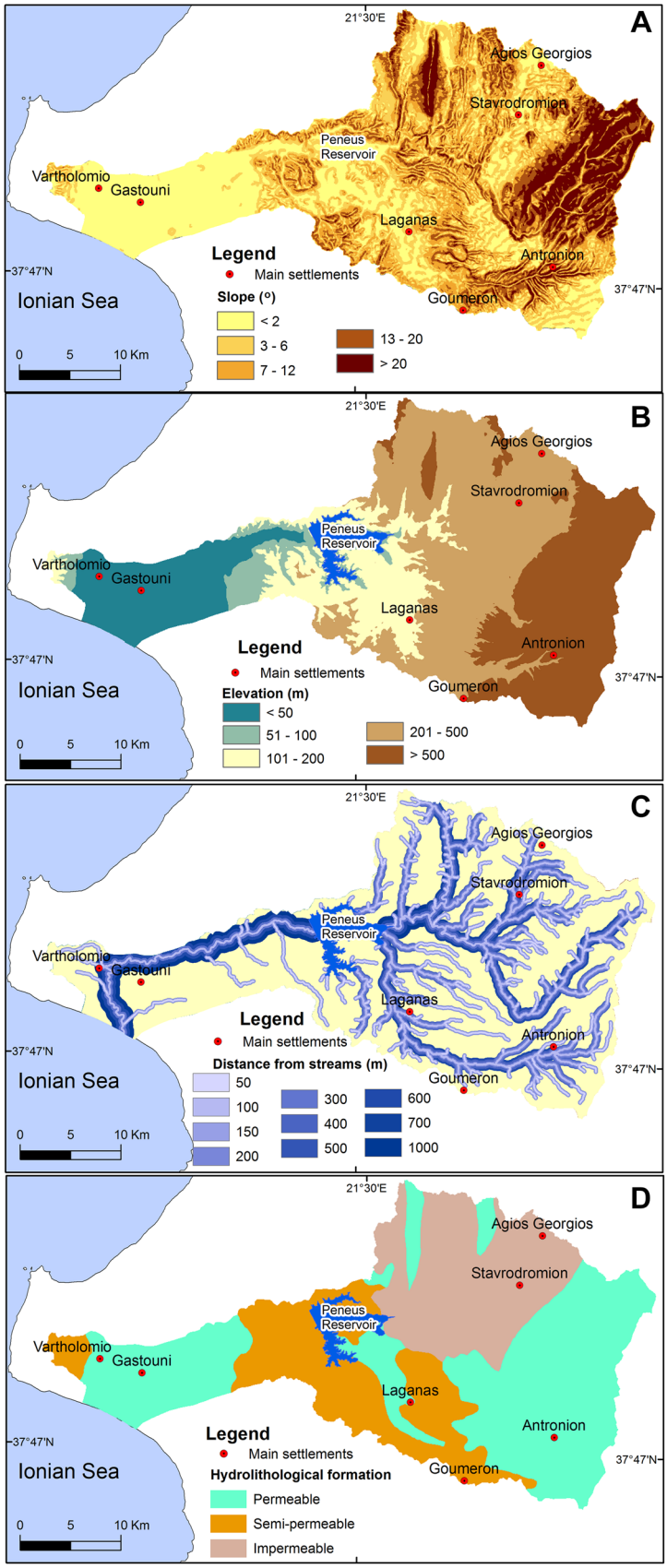

Fig. 4 Thematic maps of slope (**a**), elevation (**b**), distance from streams (**c**) and hydrolithological formations (**d**) that were used in the assessment of flood hazard

and support the occurrence of flood events (Bathrellos et al. 2018) (Fig. 4d; Table 3).

Land use We used the land use classification as depicted in Fig. 3a. According to Bathrellos et al. (2016), urban areas increase the surface runoff and create favourable conditions for flooding. Therefore, we assigned the highest rate to the urban areas (Table 3).

Similarly to the procedure described in the landslide hazard assessment section, a final 5 × 5 matrix was created after combining the five separate matrices using the average mean. This final matrix served as the input for the application of the AHP and the calculation of the final weights. The pair-wise comparisons and the weighting coefficient of each adopted factor along with the estimated CR are tabulated in Table 4. The flood hazard index (FI) was calculated by means of the weighted linear combination:

$$\mathrm{FI} = \sum_{i=1}^{n} R_i W_i,$$

where n is the number of factors, R_i is the rating of factor i and W_i is the weight of factor i.

Using the recorded flood events that are included in published works (Migiros 2010; Ministry of Environment and Energy 2017), we created a point layer with the locations where severe flood events occurred for the period from 1920 to 2012. These flood events were used for the verification of the flood hazard map and the final multi-hazard maps.

Seismic hazard assessment map

To calculate the seismic hazard assessment map, we used a pure statistical and a semi-statistical approach by means of the extreme values method (e.g., Makropoulos and Burton 1985a, b) and the Cornell approach (e.g., Papaioannou and Papazachos 2000; Tselentis and Danciu 2010), respectively. We estimated the spatial distribution of the maximum expected values of Arias intensity (Arias 1970) as well as Moment Magnitude for a return period of 475 years (i.e., 90% probability of not being exceeded in the next 50 years). To achieve a better representation of the earthquake destructiveness, we considered one ground motion parameter as well as magnitude. Additionally, as in the case of landslide and flood hazard assessment we took into account information about the geological formations and the active faults of the study area. The selection of the appropriate factors was based on previous studies, where similar approaches have been successfully applied (Bathrellos et al. 2012, 2013, 2017a; Chousianitis et al. 2016).

Arias intensity The spatial distribution of the Arias intensity values was evaluated through the Cornell (1968) approach using the Crisis2007 code (Ordaz et al. 2007). The areal source zones of shallow seismicity as developed within the framework of the SHARE project (http://www.share-eu.org), along with the Arias intensity ground motion prediction equation (GMPE) of Chousianitis et al. (2014) were incorporated in the analysis. Finally, the estimated map was subdivided into four classes, namely (a) < 0.6 m/s, (b) 0.6–0.7 m/s, and (c) 0.7–0.8 m/s and (d) > 0.8 m/s (Fig. 5a). This subdivision was chosen on the basis of the obtained range of Arias intensity values within the study area, which is above 0.5 m/s, and because Keefer and Wilson (1989) defined values of 0.32 m/s and 0.54 m/s as shaking thresholds for seismically induced coherent landslides and lateral spreads/flows respectively. Since the entire range of the obtained Arias intensity values exceeds the lower threshold of Keefer and Wilson (1989) and is almost equal to their higher threshold, we straightforwardly defined four classes every 0.1 m/s and we assigned the highest rating to the class with Arias intensity values larger than 0.8 m/s (Table 5).

Magnitude We evaluated the maximum expected earthquake magnitude by means of the zone-free approach of extreme values (i.e., Burton et al. 2003; Papadopoulou-Vrynioti et al. 2013a, b; Pavlou et al. 2013), as it is implemented in the HAZAN code (Makropoulos and Burton 1986). The epicenters and the source parameters required by the extreme values method were obtained from the SHARE earthquake catalogue. As for Arias intensity, a return period of 475 years was considered. The derived map was subdivided into the following classes: (a) < 5.5, and (b) > 5.5 (Fig. 5b), due to the fact that earthquakes below this thresh-

Table 4 Pair-wise comparisons, weights of each adopted factor in flood hazard assessment and the calculated CR value

	F1	F2	F3	F4	F5	Weights, W_i
F1	1	4	1/2	3	1/2	0.213
F2		1	1/3	1/2	1/4	0.067
F3			1	3	1	0.303
F4				1	1/3	0.261
F5					1	0.100
CR = 0.03						

F1 slope, *F2* elevation, *F3* distance from streams, *F4* hydrolithological formations, *F5* land cover

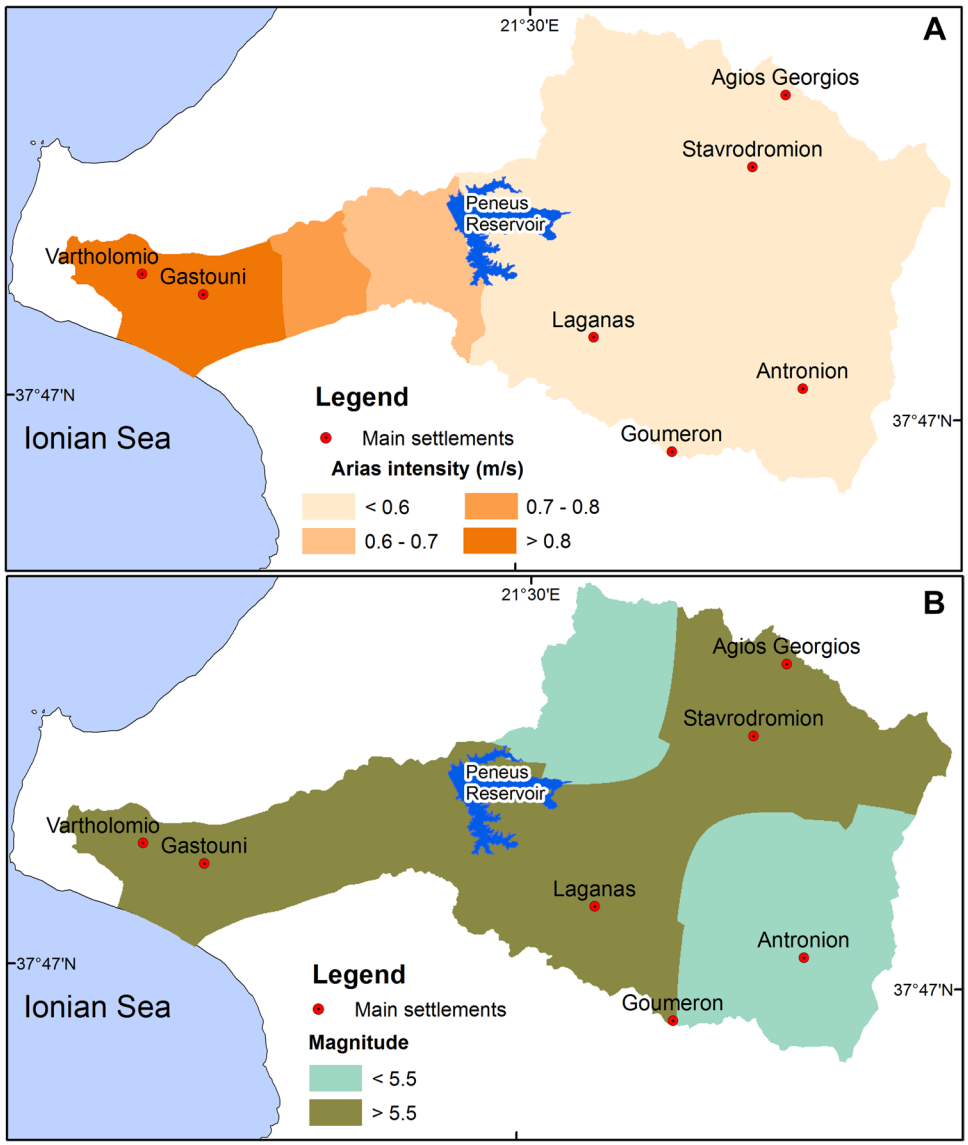

Fig. 5 Thematic maps of Arias intensity (**a**) and moment magnitude (**b**) that were used in the assessment of seismic hazard

Table 5 The factors and the classes that we considered for the assessment of seismic hazard, along with the corresponding rating for each one

Factor	Class	Rating
Arias intensity (m/s)	> 0.8	4
	0.7–0.8	3
	0.6–0.7	2
	< 0.6	1
Moment magnitude	> 5.5	4
	< 5.5	3
Lithology	Quaternary deposits, fine grained and mixed phases, and loose to coherent	3
	Quaternary coherent, coarse-grained deposits	2
	Neocene coarse-grained sediments	1
	Neocene mixed phase sediments	4
	Flysch	4
	Rocks	0
Active faults	Entire study area	4

old value cannot affect well-engineered structures. In view of that, the highest rate was assigned to the class with earthquake magnitude above 5.5 (Table 5).

Lithology We used the lithology classification as depicted in Fig. 2a for the case of landslide hazard assessment. Here we assigned the highest rate to the Neocene mixed phases sediments along with flysch due to their unstable state that has the potential to intensify the ground shaking under the influence of seismic impact and consequently increase the hazard level and related risk (Koukis and Rozos 1990) (Table 5).

Active faults Since the study area is relatively small, it becomes evident that the active faults that crosscut the broader area (Fig. 2b) will have equal impact at the drainage basin of Peneus River, and as a result we assigned the highest rating to this factor (Table 5).

Similarly to the procedure described in the landslide and flood hazard assessment sections, a final 4 × 4 matrix was created after combining the five separate matrices using the average mean. This final matrix served as the input for the application of the AHP and the calculation of the final weights. The pair-wise comparisons and the weighting coefficient of each adopted factor along with the estimated CR are tabulated in Table 6. The seismic hazard index (SI) was calculated through the equation:

$$\mathrm{SI} = \sum_{i=1}^{n} R_i W_i,$$

where n is the number of the factors, R_i is the rating of the factor i and W_i is the weight of the factor i.

Multi-hazard map for urban development

The hazard maps which we produced in the previous section followed a consistent classification into five categories. However, a simple summation of the three aforementioned hazard maps cannot be considered adequate for the production of a reliable single multi-hazard map. This can be justified by the fact that within a specific area some geohazards may emerge with different intensity and significance compared to others, as well as they can interact with each other. To overcome this difficulty, we evaluated the relative importance between the three geohazard maps via the AHP. We assigned the larger relative importance to the seismic hazard due to the fact that the study area, apart from the high seismic activity, has a rich history of earthquakes that caused secondary seismically induced phenomena and particularly landslides and in this framework this kind of hazard appears to exhibit a larger threat potential for the study area. Two of the most notorious cases were the 1993 M_L 5.2 Pyrgos earthquake which caused landslides at 47 locations and liquefaction phenomena at 7 localities in the vicinity of the epicenter (Koukouvelas et al. 1996), and the 2008 M_L 6.5 Andravida earthquake which triggered numerous environmental effects including landslides and rockfalls, surface fractures and liquefaction phenomena (Mavroulis et al. 2010). The landslide hazard ranked second in our relative comparison because the past landslide occurrences within the study area are much more numerous than the flood occurrences. In this context, the pair-wise comparisons and the weighting coefficient of each natural hazard are tabulated in Table 7.

The overall score of the multi-hazard map as regards the suitability for urban development was computed using the following equation which calculates the suitability degree (S):

$$S = \sum_{i=1}^{n} H_i W_i,$$

where n is the number of the geohazards, H_i is the geohazard i and W_i is the weight of the geohazard i.

Here we should acknowledge that uncertainties in the weights of the adopted factors have the potential to bias the outcome of every suitability assessment, and therefore, they should be taken into account for robust and reliable results. In this context, Bathrellos et al. (2013, 2016, 2017a) evaluated geo-environmental factors through the AHP method taking into account the uncertainty in the weighting

Table 6 Pair-wise comparisons, weights of each adopted factor in seismic hazard assessment and the calculated CR value

	S1	S2	S3	S4	Weights, W_i
S1	1	4	6	7	0.613
S2		1	3	4	0.224
S3			1	3	0.110
S4				1	0.056
CR = 0.03					

S1 arias intensity, *S2* moment magnitude, *S3* lithology, *S4* active faults

Table 7 Pair-wise comparisons, weights of landslide hazard (H1), flood hazard (H2) and seismic hazard (H3) along with the calculated CR

	H1	H2	H3	Weights, W_i
H1	1	3	1/2	0.332
H2		1	1/3	0.139
H3			1	0.529
CR = 0.05				

coefficients. According to this approach the error ΔS introduced by the uncertainties ΔW_i of the weighting coefficient is:

$$\Delta S = \sqrt{\sum_{i=1}^{n} (\Delta W_i X_i)^2}$$

In the present study, each coefficient was adjusted 20% from its original value, thus the uncertainties ΔW_i are 0.067 for landslide hazard, 0.028 for flood hazard, and 0.106 for seismic hazard. The error (ΔS) was calculated by applying the aforementioned equation. Next, we multiplied this value with 1.96 to compute suitability values at 95% confidence level and we finally defined their upper and lower threshold (Bathrellos et al. 2017a). Hence, three maps illustrating the suitability for urban development were produced. Finally, the existing urban areas and infrastructure of the study area were superimposed to the basic suitability map.

Results

AHP results—individual hazard assessment maps

Landslide hazard assessment map

After the application of the AHP method, we derived the landslide hazard assessment map was which is presented in Fig. 6. Using the standard deviation method which shows how much the data differs from the mean value (Standard Deviation Classification 2017), we classified the continuous numerical values of this map. Ultimately, the area was categorized into five classes, corresponding to different hazard levels, i.e., very low, low, moderate, high and very high hazard (Fig. 6). The landslide hazard analysis highlighted that the eastern, north-eastern, north-western and southern part of the study area host the most landslide-prone regions (i.e., the high and very high hazard zones).

It was justified that thirty-five (35) landslides occurred within the study area. The majority of these landslides (21 out of the 35) occurred at areas where Neocene and flysch formations outcrop. The thick weathering mantle that characterize these formations, favours the manifestation of creep movements or fast rotational slides (IUGSWGL 1995; Rozos et al. 2013). The verification of the landslide hazard assessment map was achieved by superimposing the landslide occurrences over the landslide hazard assessment map (Fig. 6). This validation revealed that 19% of landslide events are situated within the very high hazard zones, 41% into the high hazard zones, 25% into the moderate hazard zones, 13% into the low hazard zones, and 3% into the very low landslide hazard zones.

Flood hazard assessment map

Figure 7 shows the flood hazard assessment map. The study area was categorized, using the standard deviation method,

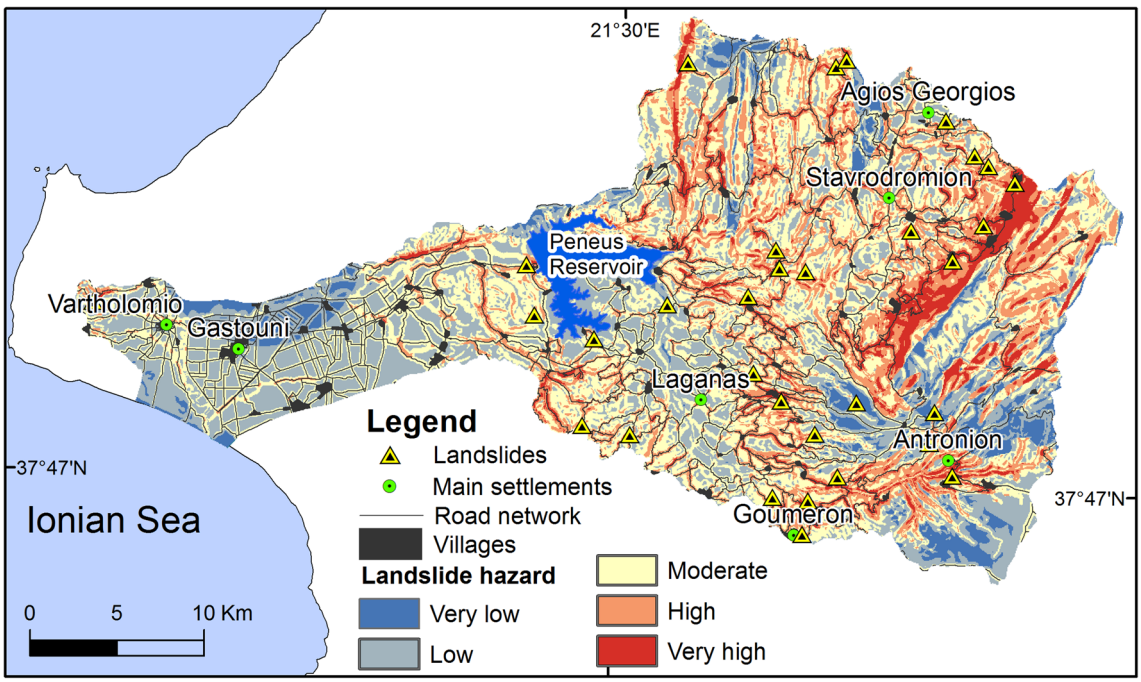

Fig. 6 Landslide hazard zonation map along with the spatial distribution of the existing landslides within the study area

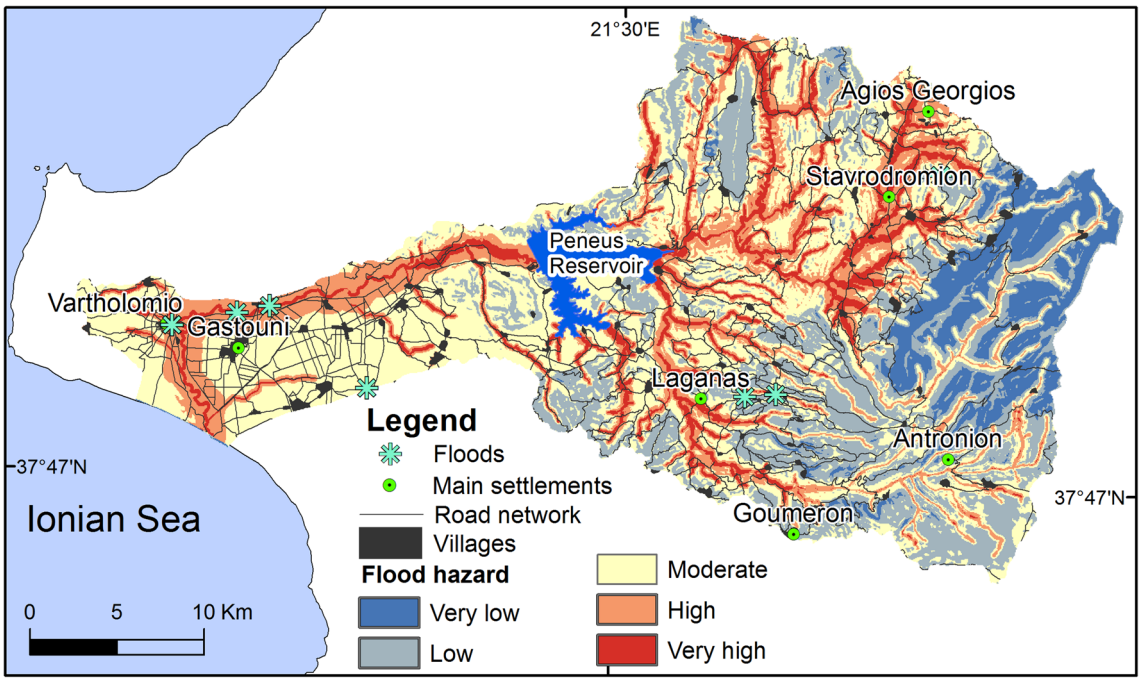

Fig. 7 Flood hazard zonation map along with the spatial distribution of recorded flood events within the study area

into five levels of flood hazard, i.e., very low, low, moderate, high and very high. It is illustrated in Fig. 7 that the prone areas (high and very high hazard zones) are located along the main stream of Peneus drainage network, i.e., in the western, northern and south-western part of the study area.

The majority of flood events are located near the towns of Vartholomio and Gastouni (Fig. 7). Among the past flood events that occurred within the study area, 50% are situated into the very high hazard zones and 30% into the high hazard zones.

Seismic hazard assessment map

As regards the seismic hazard map, the study area was categorized, using the standard deviation method, into five seismic hazard levels, i.e., very low, low, moderate, high and very high (Fig. 8). It is evident from Fig. 8 that the earthquake-prone zones are distributed in the western part of the study area.

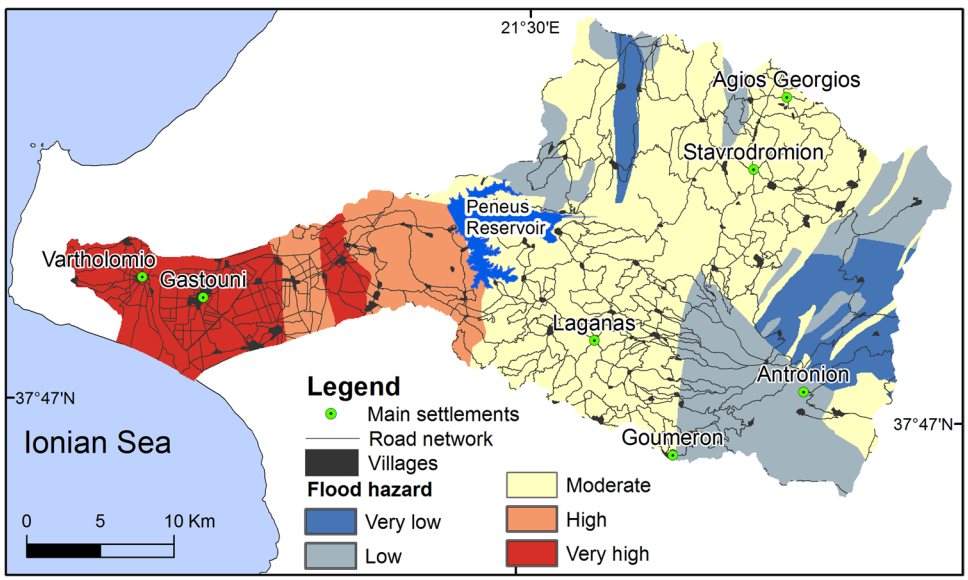

Fig. 8 The seismic hazard zonation map

Multi-hazard map for urban development

The multi-hazard analysis that we implemented in the previous section highlighted the suitable areas for urban development (Fig. 9). Three suitability maps were produced, among which one depicts the straightforward results of the AHP method, while the other two illustrate the minimum and maximum value of the suitability assessment for each pixel after taking into account the uncertainty in the weighting coefficients. The continuous values of the three suitability assessment maps were classified into five categories. The areas of high and very high suitability are situated primarily at the eastern and northern part of the study area, while the entire western part appears to be of very low suitability.

Table 8 tabulates the percentages representing the area of each suitability class with respect to the area of the basin of Peneus River for the three maps of Fig. 9. Taking as reference the values derived from the generic suitability map (S), it is observed that regarding the map showing the upper suitability values, the spatial extent of the low and very high suitability classes have been decreased, the extent of the high suitability zones remained unchanged, while the extent of the very low and moderate suitability zones have been increased. Likewise, for the map showing the lower suitability values, the area of the very low, low and high suitability classes has been decreased, whereas the spatial extent of moderate and very high zones has been increased.

Table 8 Percentages representing the area of each suitability class with respect to the entire study area for the three maps of Fig. 9

Suitability zone	S (%)	S_{max} (%)	S_{min} (%)
Very high	9	3	13
High	28	28	23
Moderate	38	45	48
Low	15	12	9
Very low	10	12	8

To validate the basic suitability map (S), we used the past landslide occurrences as well as the recorded flood events for the period 1920–2012. The validation revealed that none landslide is located within the very high suitability areas, 22% of the landslides are situated within the high suitability areas, 47% within the moderate suitability areas, 25% within the low suitability areas, and 6% within the very low suitability areas. As regards the flood events, 30% of them are located within the moderate suitability areas, 20% within the low suitability areas, and 50% within the very low suitability areas.

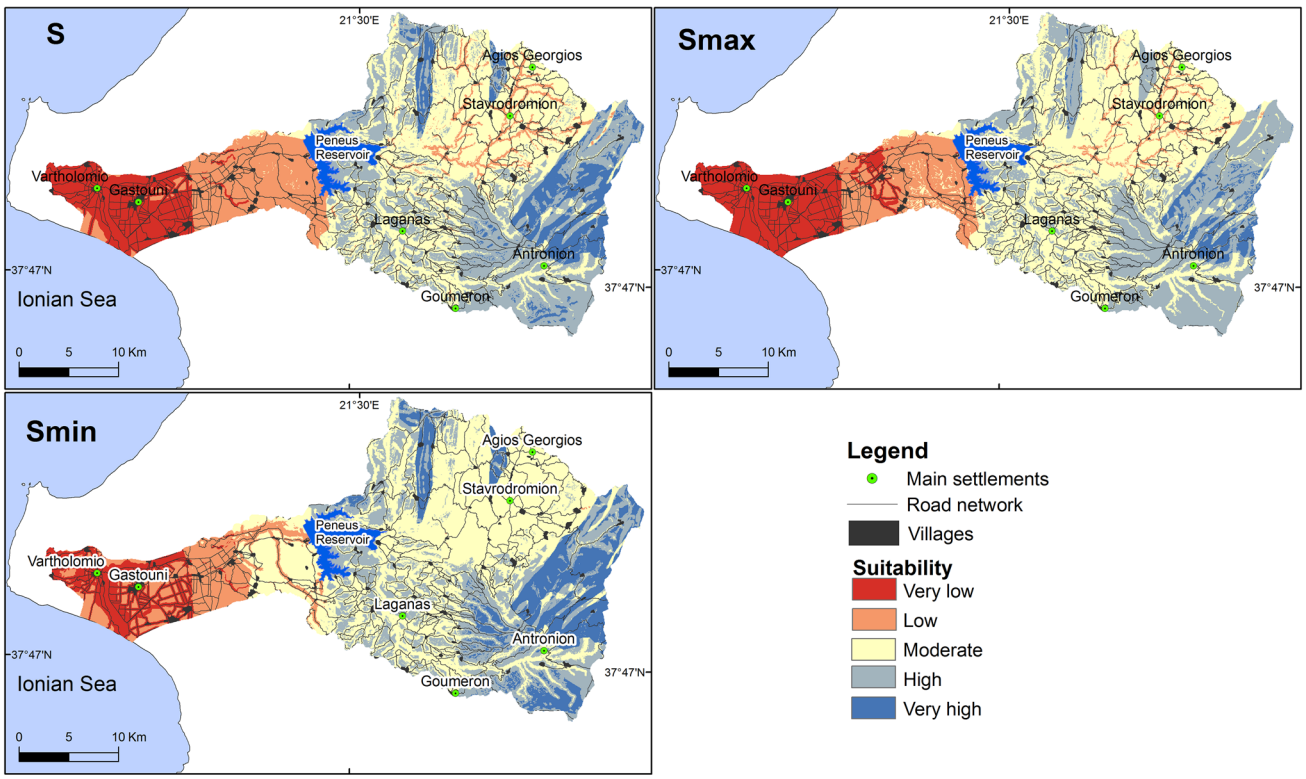

Fig. 9 Map illustrating the suitability assessment for urban development (S) along with the upper (S_{max}) and lower (S_{min}) suitability values that were obtained by accounting for the uncertainty in the weighting coefficients

Afterwards, the infrastructures and the main urban areas were superimposed to the basic suitability map (*S*). In this context, we calculated the number of settlements, the area of urban fabric and the length of the road network that falls into each suitability zone (Table 9). The results demonstrate that few settlements and a small part of the urban fabric are situated within the very high and high suitability zones. Similarly, only a small percentage of the total length of the road network is situated within areas of very high and high suitability. On the contrary, a large number of settlements, as well as large parts of the urban fabric and the road network are situated within moderate, low and very low suitability zones.

Discussion

The landslide hazard analysis highlighted that the eastern, north-eastern, north-western and southern part of the area under investigation host the most landslide-prone regions (i.e., the high and very high hazard zones). The broader area of NW Peloponnese is characterized by rather steep slopes, consists of cyclothematic formations such as flysch and Neocene sediments, as well as of loose Quaternary deposits and is controlled by active faults. Several severe landslide occurrences were triggered by heavy rainfall as well as by seismic activity (Koukouvelas and Doutsos 1997; Chalkias et al. 2016). It is worth mentioning that in 2007 extensive fires in Elis Prefecture burned more than 900 km^2 of land. Thus the extreme deforestation that took place supported by the prevailing morphological and lithological conditions and the intense tectonic activity triggered a lot of landslide phenomena within the study area (Agricultural University of Athens 2007; Migiros 2010). The validation of the result of the landslide hazard assessment highlighted that the majority of the occurred landslides (60%), are situated within the zones of high and very high hazard. Therefore, the predictive capacity of the applied method can be considered satisfactory.

As regards the flood events that occurred within the study area, Karymbalis et al. (2011) showed that in western Peloponnese apart from the heavy rainfall, the most important physical causes that are responsible for flash flood events at the lower reaches of small catchments are the geomorphic features of the drainage networks. Heavy rainfall, on bare and steeply cultivated land in the river basins of western Peloponnese, influence the volume of runoff and enhance flash floods in downstream areas (Woodward 2009). Furthermore, the overland flow on bare fire affected areas of Elis Prefecture resulted in floods near the sectors of gentle slopes located in the western part of the Prefecture (Migiros 2010). The flood-prone areas (high and very high hazard zones) are located mainly along the main stream of Peneus drainage network. A large percentage of the flood events (80%) that occurred within the study area are situated within the zones of high and very high flood hazard. The geomorphic characteristics of the drainage basin such as the morphology and the gentle slope at the lower reaches of Peneus River create favorable conditions for flooding. Apart from the physical parameters, an essential factor for the occurrence of flood phenomena is human interference. In this context, land use changes in the areas affected by the 2007 extensive fires have promoted flood events. Moreover the limited artificial riverbed at the lower reaches of Peneus River in consequence of cultivated land and urban activities, greatly burden the natural characteristics of flow and cause flooding.

The two approaches that we followed to assess the seismic hazard illustrated a moderate to high seismic potential. The main threat for the study area is the strike slip fault that produced the 8 June 2008 strong earthquake ($M_w = 6.4$). Although this event did not occurred within the limits of the study area, but a few kilometres north of its northern part, this fault constitutes a significant threat for the broader area. However, contrary to the straightforward validation of the landslide and flood hazard assessment maps, we should point out here the long debated problem and the difficulty of verifying seismic hazard estimates. Even though that some approaches have been proposed (Stirling and Petersen 2006; Mucciarelli et al. 2008; Marzocchi and Jordan 2014), the necessity of verification data that spans a very long time interval is a requirement for a reliable assessment of the seismic hazard results (cf. Iervolino 2013). The latter, however, is somewhat difficult to be accomplished. A potential solution would be the validation through the usage of macroseismic intensity. In this case however, the validation is performed by comparing numerical quantities (in our case moment magnitude and

Table 9 Number of settlements (*S*), urban fabric area (UF) and length of the road network (*R*) that fall into each suitability zone for urban development, along with the percentages (%) with respect to their total extent

Suitability zone	*S*	%	UF in Km^2	%	*R* in Km	%
Very low	17	13	4.1	28	272.4	21
Low	24	18	3.5	24	263.2	20
Moderate	56	43	6.4	44	574.7	44
High	26	20	0.3	2	171.1	13
Very high	8	6	0.4	3	28.9	2
Total	131	100	14.7	100	1310.4	100

Arias intensity) with non measurable quantities (macroseismic intensity) that describe the effect of an earthquake.

Although, individual hazard assessment maps are valuable during the early stages of urban planning, they may eventually confuse the scientists involved in the analyses if they have to deal with a large number of maps with diverse information and varied spatial covering and resolution. On the contrary, a synthesized multi-hazard map supports planners and engineers towards the implementation of sustainable urban planning by providing them homogenized information about different geohazards for a specific area. From this angle, in the present study we produced a single multi-hazard map to assist the identification of suitable areas for urban development by evaluating the relative importance between three individual hazard maps via the AHP method. We highlighted the potential suitability for urban development by dividing the study area into five classes spanning from very low to very high suitability. The eastern and northern part of the study area hosts the majority of the areas characterized by high and very high suitability, whereas the western part is dominated by areas of low and very low suitability. At this part of the study area the hazard level for the three types of geohazards that we evaluated is found to be from moderate to very high. The moderate suitability zones are mainly distributed at the north-eastern part of the study area, where the level of seismic hazard is moderate, while the landslide and flood hazard are high and very high, respectively.

The applied methodology is useful for urban suitability analysis (Bathrellos et al. 2017a), although it presents limitations as regards the calculation of uncertainties (Chen et al. 2010). This was examined by estimating two additional scenarios that show the upper and lower suitability values after accounting for the uncertainty in the weighting coefficients. The basic suitability map (S) classifies about 35% of the study area within high and very high suitability zones for urban development and 25% within low and very low suitability zones. The two additional maps that account for the uncertainty in the weighting coefficients (S_{max} and S_{min}) illustrate rather low spatial variation with respect to the basic suitability map. The common pattern between the S_{max} and S_{min} suitability maps with respect to the S map is the decrease of the low suitability zones and the increase of the moderate suitability zones.

However, it should be acknowledged that the synthesis of different hazard maps can lead to a multi-hazard map that does not takes into account the actual hazard level of a specific area (Kappes et al. 2012). So as a step forward, we validated the basic suitability assessment map by superimposing historical occurrences of landslides and floods. Almost 80% of the landslides are situated within moderate, low and very low suitability zones, while 70% of the flood events within low and very low suitability zones. Thus, the applied methodology displayed a high predictive capability and generated reliable results.

As regards the distribution of the existing settlements with respect to the areas that are depicted in the basic suitability assessment map, the majority (74%) is situated within moderate, low and very low suitability zones. In contrast, about 50% of the urban fabric and 40% of the road network is situated within low and very low suitability zones. This means that they have been constructed at areas susceptible to natural hazards. This is not surprising, since the majority of the aforementioned settlements and infrastructure have been constructed decades ago, when land use planning was almost completely absent and only socio-economic criteria were considered.

Conclusions

The applied multi-hazard analysis within the framework of the present study achieved reliable results regarding the delineation of areas that are suitable for urban development with respect to the location of the past landslide and flood events. The results highlighted that the parts of the study area which are found to be prone to natural hazards are located in the western and north-eastern part of the drainage basin of Peneus (Pinios) River (Western Peloponnesus, Greece). The produced multi-hazard map indicated that the most suitable areas for urban development are located in the eastern part of the study area, where the level of exposure to natural hazards is low and very low. Additionally, the uncertainty analysis showed insignificant variations of the spatial distribution of the suitability zones. For local scales the approach is able to identify the areas that are prone to natural hazards during the early stages of the urban development planning.

Additionally, the spatial distribution of the existent urban fabric can be analyzed towards identifying the parts that are located in unsafe areas so as to design and implement hazard mitigation measures. Within the study area, 50% of the urban areas and of the road network were found to be located within areas susceptible to natural hazards. Therefore, engineers, decision-makers and environmental managers may implement the analysis that we implemented in the present study during new or existing planning projects and produce maps that will make possible the adoption of policies and strategies towards the goal of multi-hazard mitigation.

Acknowledgements The constructive and thorough reviews of two anonymous reviewers are warmly acknowledged.

References

Abdulwahid WM, Pradhan B (2016) Landslide vulnerability and risk assessment for multi-hazard scenarios using airborne laser scanning data (LiDAR). Landslides 14(3):1057–1076

Agricultural University of Athens (A.U.A.) (2007) Study on the rehabilitation and development of the agricultural sector—forestry & environmental protection in fire affected areas Elis prefecture. AUA, for the Ministry of Rural Development and Food, Athens, 320

Althuwaynee OF, Pradhan B (2016) Semi quantitative landslide risk assessment at Kuala Lumpur Metropolitan City using GIS and exposure based analysis. Geomat Nat Haz Risk 8(2):706–732

Arias A (1970) A measure of earthquake intensity. In: Hansen RJ (ed) Seismic design for nuclear power plants. MIT Press, Cambridge, pp 438–483

Ayalew L, Yamagishi H (2005) The application of GIS-based logistic regression for landslide susceptibility mapping in the Kakuda-Yahiko Mountains, Central Japan. Geomorphology 65:15–31

Baja S, Chapman DM, Dragovich D (2007) Spatial based compromise programming for multiple criteria decision making in land use planning. Environ Model Assess 12(3):171–184

Bathrellos GD, Skilodimou HD, Kelepertsis A, Alexakis D, Chrisanthaki I, Archonti D (2008) Environmental research of groundwater in the urban and suburban areas of Attica region, Greece. Environ Geol 56(1):11–18

Bathrellos GD, Kalivas DP, Skilodimou HD (2009) GIS-based landslide susceptibility mapping models applied to natural and urban planning in Trikala, Central Greece. Estud Geol-Madrid 65(1):49–65

Bathrellos GD, Gaki-Papanastassiou K, Skilodimou HD, Papanastassiou D, Chousianitis KG (2012) Potential suitability for urban planning and industry development by using natural hazard maps and geological—geomorphological parameters. Environ Earth Sci 66(2):537–548

Bathrellos GD, Gaki-Papanastassiou K, Skilodimou HD, Skianis GA, Chousianitis KG (2013) Assessment of rural community and agricultural development using geomorphological–geological factors and GIS in the Trikala prefecture (Central Greece). Stoch Environ Res Risk Assess 27(2):573–588

Bathrellos GD, Skilodimou HD, Maroukian H (2014) The spatial distribution of Middle and Late Pleistocene cirques in Greece. Geogr Ann A 96(3):323–338

Bathrellos GD, Karymbalis E, Skilodimou HD, Gaki-Papanastassiou K, Baltas EA (2016) Urban flood hazard assessment in the basin of Athens Metropolitan city, Greece. Environ Earth Sci 75(4):319

Bathrellos GD, Skilodimou HD, Chousianitis K, Youssef AM, Pradhan B (2017a) Suitability estimation for urban development using multi-hazard assessment map. Sci Total Environ 575:119–134

Bathrellos GD, Skilodimou HD, Maroukian H (2017b) The significance of tectonism in the glaciations of Greece. In: Hughes PD, Woodward JC (eds) Quaternary glaciation in the Mediterranean mountains. Geological Society Special Publication, London, Vol. 433, pp 237–250

Bathrellos GD, Skilodimou HD, Maroukian H, Gaki-Papanastassiou K, Kouli K, Tsourou T, Tsaparas N (2017c) Pleistocene glacial and lacustrine activity in the southern part of Mount Olympus (central Greece). Area 49(2):137–147

Bathrellos GD, Skilodimou HD, Soukis K, Koskeridou E (2018) Temporal and spatial analysis of flood occurrences in drainage basin of Pinios River (Thessaly, central Greece). Land 7(3):106. https://doi.org/10.3390/land7030106

Bender S (1991) Primer on natural hazard management in integrated regional development planning. Department of Regional Development and Environment, Executive Secretariat for Economic and Social Affairs, Organization of American States, Washington

Burton PW, Xua Y, Tselentis GA, Sokos E, Aspinall W (2003) Strong ground acceleration seismic hazard in Greece and neighboring regions. Soil Dyn Earthq Eng 23:159–181

Chalkias C, Polykretis C, Ferentinou M, Karymbalis E (2016) Integrating expert knowledge with statistical analysis for landslide susceptibility assessment at regional scale. Geosciences 6(1):14

Chen Y, Yu J, Khan S (2010) Spatial sensitivity analysis of multicriteria weights in GIS-based land suitability evaluation. Environ Modell Softw 25:1582–1591

Chousianitis K, Del Gaudio V, Kalogeras I, Ganas A (2014) Predictive model of Arias intensity and Newmark displacement for regional scale evaluation of earthquake-induced landslide hazard in Greece. Soil Dyn Earthq Eng 65:11–29

Chousianitis K, Del Gaudio V, Sabatakakis N, Kavoura K, Drakatos G, Bathrellos GD, Skilodimou HD (2016) Assessment of earthquake-induced landslide hazard in Greece: from Arias intensity to spatial distribution of slope resistance demand. B Seismol Soc Am 106(1):174–188

Copernicus (2016) Copernicus land monitoring service. Available at http://land.copernicus.eu. Accessed 06 July 2016

Cornell CA (1968) Engineering seismic risk analysis. B Seismol Soc Am 58:1583–1606

Das HO, Sonmez C, Gokceoglu C, Nefeslioglu HA (2013) Influence of seismic acceleration on landslide susceptibility maps: a case study from NE Turkey (the Kelkit Valley). Landslides 10(4):433–454

De Moel H, van Alphen J, Aerts JCJH (2009) Flood maps in Europe-methods, availability and use. Nat Hazards Earth Syst Sci 9(2):289–301

Earthquake Planning and Protection Organization (EPPO) (2003) New national seismic hazard map. National Gazette, 1154, vol B

ECI (2004) Expert Choice Inc. http://www.expertchoice.com. Accessed 08 Sept 2016

El Morjani Z, Ebner S, Boos J, Abdel Ghaffar E, Musani A (2007) Modelling the spatial distribution of five natural hazards in the context of the WHO/EMRO Atlas of disaster risk as a step towards the reduction of the health impact related to disasters. Int J Health Geogr 6:1–28

Federal Emergency Management Agency (F.E.M.A.) (2004) Using HAZUS-MH for risk assessment. HAZU-MH risk assessment and user group series. FEMA 433

Fernández DS, Lutz MA (2010) Urban flood hazard zoning in Tucumán Province, Argentina, using GIS and multicriteria decision analysis. Eng Geol 111(1–4):90–98

Goldsworthy M, Jackson J (2001) Migration of activity within normal fault systems: examples from the Quaternary of mainland Greece. J Struct Geol 23(2):489–506

Goldsworthy M, Jackson J, Haines AJ (2002) The continuity of active fault systems in Greece. Geophys J Int 148:596–618

Hellenic Army Geographical Service (H.A.G.S) (1989) Topographic maps (scale 1:50,000), Athens

Hopkins LD (1977) Methods for generating land suitability maps: a comparative evaluation. J Am Inst Planners 43(4):386–400

Iervolino I (2013) Probabilities and fallacies: why hazard maps cannot be validated by individual earthquakes. Earthq Spectra 29(3):1125–1136

Institute of Geology and Mineral Exploration (I.G.M.E) (1983) Geological map of Greece (Scale 1:50,000), Athens

Institute of Geology and Mineral Exploration (I.G.M.E.) (1993) Engineering Geological map of Greece (Scale 1:500,000), Athens

IUGSWGL (International Union of Geological Sciences Working Group on Landslides) (1995) A suggested method for describing the rate of movement of a landslide. Bull IAEG 52:75–78

Jebur MN, Pradhan B, Shafri HZM, Yusof Z, Tehrany MS (2015) An integrated user-friendly ArcMAP tool for bivariate statistical modeling in geoscience applications. Geosci Model Dev 8:881–891

Kamberis E, Bathrellos GD, Kokinou E, Skilodimou HD (2012) Correlation between the structural pattern and the development of the hydrographic network in a portion of Western Thessaly basin (Greece). Cent Eur J Geosci 4(3):416–424

Kappes M, Papathoma-Kohle M, Keiler M (2011) Assessing physical vulnerability for multi-hazards using an indicator-based methodology. Appl Geogr 32:577–590

Kappes MS, Keiler M, von Elverfeldt K, Glade T (2012) Challenges of analyzing multi-hazard risk: a review. Nat Hazards 64(2):1925–1958

Karaman H, Erden T (2014) Net earthquake hazard and elements at risk (NEaR) map creation for city of Istanbul via spatial multi-criteria decision analysis. Nat Hazards 73(2):685–709

Karymbalis E, Chalkias C, Ferentinou M, Maistrali A (2011) Flood hazard evaluation in small catchments based on quantitative geomorphology and GIS modeling: the case of Diakoniaris torrent (W. Peloponnese, Greece). In: Lamprakis N, Stournaras G, Katsanou K (eds) Advances in the research of aquatic environment. Springer, Berlin, pp 137–145

Keefer DK, Wilson RC (1989) Predicting earthquake induced landslides with emphasis on arid or semi-arid environments. In: Sadler PM, Morton DM (eds) Landslides in a semi-arid environment, inland geological society, vol 2. Inland Geological Society, Riverside, pp 118–149

Kokinou E, Skilodimou HD, Bathrellos GD, Antonarakou A, Kamberis E (2015) Morphotectonic analysis, structural evolution/pattern of a contractional ridge: Giouchtas Mt., Central Crete, Greece. J Earth Syst Sci 124(3):587–602

Koukis G, Rozos D (1990) Geotechnical properties of the Neogene sediments in the NW Peloponnesus, Greece. In: Proceedings of the 6th international congress of IAEG. Balkema, Rotterdam, pp 405–412

Koukouvelas IK, Doutsos T (1997) The effects of active faults on the generation of landslides in NW Peloponnese, Greece. In: Marinos PG, Koukis GC, Tsiambaos GC, Stournaras GC (Eds) Engineering geology and the environment, vol. 1, Balkema, Amsterdam, pp 799–804

Koukouvelas I, Mpresiakas A, Sokos E, Doutsos T (1996) The tectonic setting and earthquake ground hazards of the 1993 Pyrgos earthquake, Peloponnese, Greece. J Geol Soc London 153:39–49

Makropoulos KC, Burton PW (1985a) Seismic hazard in Greece. I: magnitude recurrence. Tectonophysics 117:205–257

Makropoulos KC, Burton PW (1985b) Seismic Hazard in Greece II: ground Acceleration. Tectonophysics 117:259–294

Makropoulos KC, Burton PW (1986) "HAZAN": A Fortan program to evaluate seismic-hazard parameters using Gumbel's theory of extreme value statistics. Comput Geosci 12(1):29–46

Marzocchi W, Jordan TH (2014) Testing for ontological errors in probabilistic forecasting models of natural systems. Proc Natl Acad Sci USA 111(33):11973–11978

Mavroulis S, Fountoulis I, Lekkas E (2010) Environmental effects caused by the Andravida (08-06-2008, ML = 6.5, NW Peloponnese, Greece) earthquake. In: Williams A, Pinches G, Chin C, McMorran T, Massey C (eds) Geologically active: 11th IAEG Congress. Taylor & Francis Group, Auckland, pp 451–459

Merwade V, Cook A, Coonrod J (2008) GIS techniques for creating river terrain models for hydrodynamic modeling and flood inundation mapping. Environ Modell Softw 23:1300–1311

Migiros G (2010) Reconstruction of Land Improvement Organisms, Prefecture of Eleia (Peneus—Alfios), Region of Western Greece. Technical Report on Water Resources Management, 129 pp

Migiros G, Bathrellos GD, Skilodimou HD, Karamousalis T (2011) Pinios (Peneus) River (Central Greece): hydrological–geomorphological elements and changes during the Quaternary. Cent Eur J Geosci 3(2):215–228

Ministry of Environment and Energy (2017) Floods, historic floods. http://www.ypeka.gr/Default.aspx?tabid=252&language=el-GR. Accessed 05 Dec 2017

Mucciarelli M, Albarello D, D'Amico V (2008) Comparison of probabilistic seismic hazard estimates in Italy. Bull Seismol Soc Am 98:2652–2664

Nefeslioglu HA, Sezer EA, Gokceoglu C, Ayas Z (2013) A modified analytical hierarchy process (M-AHP) approach for decision support systems in natural hazard assessments. Comput Geosci 59:1–8

Ordaz M, Aguilar A, Arboleda J (2007) CRISIS2007: Program for computing seismic hazard, v. 5.1. Instituto de Ingenieria, UNAM, Mexico

Panagopoulos G, Bathrellos G, Skilodimou H, Martsouka F (2012) Mapping Urban Water Demands Using Multi-Criteria Analysis and GIS. Water Resour Manag 26:1347–1363

Papadopoulou-Vrynioti K, Bathrellos GD, Skilodimou HD, Kaviris G, Makropoulos K (2013a) Karst collapse susceptibility mapping considering peak ground acceleration in a rapidly growing urban area. Eng Geol 158:77–88

Papadopoulou-Vrynioti K, Alexakis D, Bathrellos GD, Skilodimou HD, Vryniotis D, Vasiliades E, Gamvroula D (2013b) Distribution of trace elements in stream sediments of Arta plain (western Hellas): The influence of geomorphological parameters. J Geochem Explor 134:17–26

Papadopoulou-Vrynioti K, Alexakis D, Bathrellos GD, Skilodimou HD, Vryniotis D, Vassiliades E (2014) Environmental research and evaluation of agricultural soil of the Arta plain, western Hellas. J Geochem Explor 136:84–92

Papaioannou CA, Papazachos BC (2000) Time-independent and time-dependent seismic hazard in Greece based on seismogenic sources. B Seismol Soc Am 90:22–33

Pavlou K, Kaviris G, Chousianitis K, Drakatos G, Kouskouna V, Makropoulos K (2013) Seismic hazard assessment in Polyphyto Dam area (NW Greece) and its relation with the "unexpected" earthquake of 13 May 1995 (Ms = 6.5, NW Greece). Nat Hazard Earth Sys 13:141–149

Peng SH, Shieh MJ, Fan SY (2012) Potential Hazard Map for Disaster Prevention Using GIS-Based Linear Combination Approach and Analytic Hierarchy Method. J Geogr Inf Syst 4:403–411

Pham BT, Pradhan B, Bui DT, Prakash I, Dholakia MB (2016) A comparative study of different machine learning methods for landslide susceptibility assessment: A case study of Uttarakhand area (India). Environ Modell Softw 84:240–250

Pourghasemi HR, Pradhan B, Gokceoglu C (2012) Application of fuzzy logic and analytical hierarchy process (AHP) to landslide susceptibility mapping at Haraz watershed, Iran. Nat Hazards 63(2):965–996

Rahmati O, Zeinivand H, Besharat M (2016) Flood hazard zoning in Yasooj region, Iran, using GIS and multi-criteria decision analysis. Geomat Nat Haz Risk 7(3):1000–1017

Rozos D, Bathrellos GD, Skilodimou HD (2011) Comparison of the implementation of Rock Engineering System (RES) and Analytic Hierarchy Process (AHP) methods, based on landslide susceptibility maps, compiled in GIS environment. A case study from the Eastern Achaia County of Peloponnesus, Greece. Environ Earth Sci 63(1):49–63

Rozos D, Skilodimou HD, Loupasakis C, Bathrellos GD (2013) Application of the revised universal soil loss equation model on landslide prevention. An example from N. Euboea (Evia) Island, Greece. Environ Earth Sci 70(7):3255–3266

Saaty TL (1977) A scaling method for priorities in hierarchical structures. J Math Psychol 15(3):234–281

Saaty TL (1990) How to make a decision: The Analytic Hierarchy Process. Eur J Oper Res 48(1):9–26
Saaty TL (2004) Decision making – The Analytic Hierarchy and Network Processes (AHP/ANP). J Syst Sci Syst Eng 13(1):1–35
Saaty TL (2006) Rank from comparisons and from ratings in the analytic hierarchy/ network processes. Eur J Oper Res 168:557–570
Schmidt J, Matcham I, Reese S, King A, Bell R, Henderson R, Smart G, Cousins J, Smith W, Heron D (2011) Quantitative multi-risk analysis for natural hazards: a framework for multi-risk modelling. Nat Hazards 58(3):1169–1192
Setianto A, Triandini T (2013) Comparison of kriging and inverse distance weighted (IDW) interpolation methods in lineament extraction and analysis. J SE Asian Appl Geol 5(1):21–29
Skilodimou H, Livaditis G, Bathrellos G, Verikiou–Papaspiridakou E (2003) Investigating the flooding events of the urban regions of Glyfada and Voula, Attica, Greece: a contribution to Urban Geomorphology. Geogr Ann A 85(2):197–204
Skilodimou HD, Bathrellos GD, Maroukian H, Gaki-Papanastassiou K (2014) Late Quaternary evolution of the lower reaches of Ziliana stream in south Mt. Olympus (Greece). Geogr Fis Din Quat 37(1):43–50
Skilodimou HD, Bathrellos GD, Koskeridou E, Soukis K, Rozos D (2018) Physical and anthropogenic factors related to landslide activity in the Northern Peloponnese, Greece. Land 7(3):85. https://doi.org/10.3390/land7030085
Slaymaker O (1997) Geomorphic hazards. Wiley, Hoboken, 204 p
Standard Deviation Classification (2017) GIS dictionary. http://support.esri.com/en/knowledgebase/GISDictionary/term/standard%20deviation%20classification. Accessed 05 Oct 2017
Stefanidis S, Stathis D (2013) Assessment of flood hazard based on natural and anthropogenic factors using analytic hierarchy process (AHP). Nat Hazards 68:569–585
Stirling MW, Petersen M (2006) Comparison of the historical record of earthquake hazard with seismic-hazard models for New Zealand and the continental United States. B Seismol Soc Am 96(6):1978–1994
Strahler A (1957) Quantitative analysis of watershed Geomorphology. Eos Trans AGU 38(6):913–920
Svoray T, Bar (Kutiel) P, Bannet T (2005) Urban land-use allocation in a Mediterranean ecotone: habitat Heterogeneity Model incorporated in a GIS using a multi-criteria mechanism. Landsc Urban Plan 72:337–351
Tehrany MS, Pradhan B, Mansor S, Ahmad N (2015) Flood susceptibility mapping using GIS-based support vector machine model with different kernel types. Catena 125:91–101
Thapa RB, Murayama Y (2008) Land evaluation for peri-urban agriculture using analytical hierarchical process and geographic information system techniques: a case study of Hanoi. Land Use Policy 25(2):225–239
Tselentis GA, Danciu L (2010) Probabilistic seismic hazard assessment in Greece—Part I: engineering ground motion parameters. Nat Hazard Earth Syst 10:25–39
Tsolaki-Fiaka S, Bathrellos GD, Skilodimou HD (2018) Multi-criteria decision analysis for an abandoned quarry in the Evros Region (NE Greece). Land 7(2):43
Woodward J (2009) The physical geography of the Mediterranean, vol. 8. Oxford University Press, Oxford
Youssef AM, Pradhan B, Tarabees E (2011) Integrated evaluation of urban development suitability based on remote sensing and GIS techniques: contribution from analytic hierarchy process. Arab J Geosci 4(3):463–473
Youssef AM, Pradhan B, Al-Kathery M, Bathrellos GD, Skilodimou HD (2015) Assessment of rockfall hazard at Al-Noor Mountain, Makkah city (Saudi Arabia) using spatio-temporal remote sensing data and field investigation. J Afr Earth Sci 101:309–321
Youssef AM, Sefry SA, Pradhan B, Al Fadail EA (2016) Analysis on causes of flash flood in Jeddah city (Kingdom of Saudi Arabia) of 2009 and 2011 using multi-sensor remote sensing data and GIS. Geomat Nat Haz Risk 7(3):1018–1042